HHS Public Access

Author manuscript

Retin Cases Brief Rep. Author manuscript; available in PMC 2022 November 01.

Published in final edited form as:

Retin Cases Brief Rep. 2021 November 01; 15(6): 694–701. doi:10.1097/ICB.0000000000000891.

ENHANCED S-CONE SYNDROME: VISUAL FUNCTION, CROSS-SECTIONAL IMAGING, AND CELLULAR STRUCTURE WITH ADAPTIVE OPTICS OPHTHALMOSCOPY

Michael J. Ammar, MD[*], **Kurt T. Scavelli, MD**[*], **Katherine E. Uyhazi, MD, PhD**[*], **Emma C. Bedoukian, MS**[†], **Leona W. Serrano, BS**[*], **Ilaina D. Edelstein, BA**[*], **Grace Vergilio, BA**[*], **Robert F. Cooper, PhD**[*], **Jessica I. W. Morgan, PhD**[*,‡], **Priyanka Kumar, MD**[†], **Tomas S. Aleman, MD**[*,†,‡]

[*]Scheie Eye Institute

[†]The Children's Hospital of Philadelphia

[‡]the Center for Advanced Retinal and Ocular Therapeutics (CAROT), Perelman School of Medicine, University of Pennsylvania, Philadelphia, Pennsylvania

Abstract

Purpose: To describe in detail the phenotype of a patient with enhanced S-cone syndrome.

Methods: We describe a 13-year-old boy who presented with blurred vision, vitreous cells, cystoid macular edema refractory to steroid treatment, and a negative uveitic workup. The patient underwent a complete ophthalmic examination, full-field electroretinograms (ffERG), automatic static perimetry and multimodal imaging with spectral domain optical coherence tomography, and adaptive optics scanning laser ophthalmoscopy (AOSLO).

Results: Spectral domain optical coherence tomography demonstrated cystoid macular edema and a hyperthick, delaminated midperipheral retina. Fluorescein angiography did not demonstrate macular leakage. Rod-mediated ffERGs were undetectable, and there was a supernormal response to short-wavelength stimuli compared with photopically matched longer wavelengths of light consistent with enhanced S-cone syndrome. Gene screening was positive for compound heterozygous mutations *NR2E3*: a known (c.119-2 A>C) and a novel (c.119-1G>A) mutation. By perimetry, sensitivities were normal or above normal for short-wavelength stimuli; there was no detectable rod-mediated vision. AOSLO demonstrated higher than normal cone densities in the perifoveal retina and evidence for smaller outer segment cone diameters.

Conclusion: Evidence for supernumerary cones (at least twice the normal complement) by AOSLO and spectral domain optical coherence tomography was associated with supernormal S-cone sensitivities and electroretinogram responses confirming previous in vivo findings in postmortem human specimens. Smaller than normal cones in enhanced S-cone syndrome may represent "hybrid" photoreceptors analogous to the *rd7/rd7* murine model of the disease.

Reprint requests: Tomas S. Aleman, MD, Department of Ophthalmology, Scheie Eye Institute, University of Pennsylvania, 51 N. 39th Street, Philadelphia, PA 19104; aleman@pennmedicine.upenn.edu.

J. I. W. Morgan is an inventor on US Patent 8226236. The remaining authors have any financial/conflicting interests to disclose.

Keywords

ESCS; retinal degeneration; uveitis; adaptive optics; NR2E3; NRL

The enhanced S-cone syndrome (ESCS) is an infrequent, typically autosomal recessive retinal degeneration characterized by early onset of nyctalopia and supernormal S-cone function. The condition is caused by mutations in *NR2E3* (*retinal nuclear receptor subfamily, group E, member 3*), a gene that encodes a transcription factor that directs retinal photoreceptor precursors toward a rod lineage.[1–4] A minority of autosomal recessive cases have been reported in association with mutations in *NRL* (*neural retina leucine zipper*), a transcription factor upstream of *NR2E3*.[5] Many of these patients are relatively asymptomatic at an early age without obvious fundus findings but eventually present with nyctalopia, central vision loss, or visual field defects.[1,6–8] Although the fundus findings may be subtle, patients often present with a clumped pigmentary midperipheral retinopathy, pericentral degeneration, whitish yellow dots, central and peripheral retinoschisis, and cystoid macular edema (CME), which have been grouped along vitreal changes as the Goldmann-Favre syndrome.[1,7,9–13] Infrequent findings include subretinal fibrosis, choroidal neovascularization, vascular anomalies with exudation, and torpedo-like lesions.[14] Although variability in severity and phenotypic expression is well recognized, abnormalities of the electroretinogram (ERG) in this condition are pathognomonic, consisting of absent rod-mediated responses with counterintuitively large dark-adapted a-waves to high-intensity stimulation that change minimally with light adaptation and a spectral signature that indicates the responses are S-cone driven.[1,9,14,15] Retinal imaging demonstrates in most cases a delaminated, thick retina, also characteristic of this condition.[16]

Enhanced S-cone syndrome, and by extension the larger group of inherited retinal degenerations (IRDs), should be considered a diagnostic possibility in any patient with a presumed intermediate uveitis of unclear etiology that is irresponsive to conventional treatment, particularly in young patients when clinical findings may be subtle.[17] In this study, we describe details of the disease that help guide the diagnosis and detail the early functional abnormalities in this condition correlated with the underlying retinal structure, both in cross-section with spectral domain optical coherence tomography (SD-OCT), and with adaptive optics scanning laser ophthalmoscopy (AOSLO).

Methods

Informed assent and permission were obtained from the patient and his family; the procedures adhered to the Declaration of Helsinki, and the study was approved by the institutional review board. The patient underwent a complete ophthalmic examination. Automated static perimetry was performed with a modified Humphrey Field Analyzer (HFA II-i; Carl Zeiss Meditec, Dublin, CA) using a 200-ms-long, 1.7° diameter stimuli presented at 2° intervals along a horizontal profile that extended to 30° of eccentricity. Light-adapted perimetry was performed with an achromatic stimulus on a white (10 $cd \cdot m^{-2}$) background and with a short-wavelength (SW) (440-nm) stimulus on a yellow (530 nm, 100 $cd \cdot m^{-2}$) background; two-color dark-adapted perimetry was performed with 500-nm

and 650-nm stimuli. The sensitivity profile corresponds to the retinal region scanned with SD-OCT. Spectral sensitivity differences in the dark-adapted state were used to define photoreceptor mediation of the stimuli.[18] A standard full-field electroretinogram (ffERG) was recorded using a computer-based system (Espion e^3; Diagnosys LLC, Littleton, MA). Rod-mediated responses were elicited with a dim white flash (0.01 phot-cd·s·m^{-2}). A white flash (3 phot-cd·s·m^{-2}) in the dark-adapted state was used to evoke a combined rod–cone response and in light-adapted conditions in response to a 1-Hz or 30-Hz flicker to elicit cone-mediated ERGs. Light-adapted ERGs were also obtained with long-wavelength (637-nm) and SW (467-nm) stimuli photopically matched in normal subjects for L-M cone stimulation. Spectral domain OCT, en face near-infrared (NIR) reflectance (REF), and fundus autofluorescence imaging using NIR and SW excitation lights were performed using a Spectralis-HRA system (Heidelberg Engineering GmbH, Heidelberg, Germany). Segmentation of the SD-OCT images was performed with the built-in segmentation software of the Spectralis-HRA system ensuring correct identification of retinal boundaries. The custom AOSLO system used in this study and adaptive optics image analysis methods have been previously described.[19] The patient was aligned to the AOSLO system using a dental impression. Wavefront sensing was performed using an 848-nm superluminescent diode with a full width at half-maximum bandwidth (FWHM) of 26 nm (Superlum, Diodes Ltd., Cork, Ireland), and aberration correction was provided by a 97 actuator deformable mirror (Alpao SAS, Montbonnot-Saint-Martin, France). Confocal images were acquired at 16.7 frames per second over a 1° by 1° field of view using a superluminescent diode centered at 795 nm with FWHM of 15.3 nm (Superlum) and a photomultiplier tube (PMT; Hamamatsu Photonics K.K., Hamamatsu City, Japan). The patient was instructed to fixate (using the imaged eye) at a target while the AOSLO image sequences were acquired along the temporal meridian. A custom strip-registration algorithm was used for intraframe strip-based registration and dewarping of the AOSLO images. Reference frames for registration were chosen manually from the confocal image sequence, and 50 frames of the confocal AOSLO images were registered and averaged. Averaged images were then automatically montaged using a previously described algorithm. Regions of interest were extracted at 0.8 mm and 1.9 mm temporal to the fovea. Cones were identified within the regions of interest in a semiautomated fashion, using a previously described algorithm, and bound cone density was extracted from the cone locations.

Case Report

A 13-year-old hyperopic boy (spherical equivalent +2.00 in the right eye and +2.25 in the left eye) was referred for a second opinion for decreased visual acuity (20/30 in the right eye, 20/50 in the left eye), bilateral vitreous cells, and CME. He had been initially started on topical prednisolone 1% four times a day in both eyes without improvement. A comprehensive inflammatory and infectious workup was negative with the exception of HLA-B27 positivity. He had no arthralgias, and a rheumatologic evaluation was unremarkable. Fluorescein angiography showed questionable peripheral leakage in both eyes but no macular leakage. He had previously been switched from topical prednisolone to difluprednate 0.05% every 2 hours without improvement, and then started on a taper of 60-mg oral prednisone; however, he still showed no improvement. Our initial

examination revealed unchanged visual acuities, mostly pigmented vitreous cells and CME (Figure 1). With the exception of central cystoid changes, his disk, vessels, and macula were unremarkable (Figure 1). Near-infrared FAF (NIR-FAF) demonstrated an area of hyperautofluorescence just peripheral to the vascular arcades that contrasted against the unrevealing fundus appearance (Figure 1, *arrows*). Spectral domain OCT showed a thick retina near the fovea in association with the cystoid changes. Central subfield thickness was 349 μm in the right eye and 541 μm in the left eye. But unlike normal retinas, where some reduction in overall thickness is expected with increasing eccentricity, the retinal thickness topography continued to be hyperthick (>400 μm), most obvious in the peripapillary nasal retina (Figure 1C).

Hallmark Signs of Enhanced S-Cone Syndrome

Spectral domain OCT, 16.4 mm-long, cross-sections extending from the fovea into nasal midperipheral retina show hyporeflective spaces within the inner retina in both eyes (Figure 2A, asterisks) and markedly increased total retinal thickness (Figure 2A). The outer nuclear layer (ONL) was clearly visible within the macula. Nasal to the optic nerve, the retina is twice the normal thickness and acquires a “bilaminar” appearance with a discernible ONL but a thickened inner retina where the inner nuclear layer and ganglion cell layer are not easily distinguishable and is crisscrossed by highly reflective dots (Figure 2A). There are no cystoid spaces in the extrafoveal retina. In the peripapillary retina, there is approximation of the external limiting membrane to the apical retinal pigment epithelium, and the inner segment/outer segment junction band near the inner segment ellipsoid (ISe) is fragmented; the interdigitation band (IZ) is no longer discernible (Figure 2A). With increasing eccentricity into the nasal retina, there is disappearance of the ISe band followed by the external limiting membrane. The retina takes on a “bilaminar” appearance with an inner thick hyperreflective band and an outer hyporreflective band that may represent an amalgamate of nuclei from the inner nuclear layer and ONL.[16,20] Superficially, there is a thick vitreal band and numerous vitreous opacities. Full-field electroretinograms showed nondetectable rod responses. Electroretinograms recorded with a brighter stimulus that normally elicits mixed cone–rod responses in the dark-adapted state showed a peculiar morphology that closely resembled the light-adapted ERGs recorded with the same stimulus (1 Hz cone ERG) (Figure 2B). Electroretinograms recorded with SW and long-wavelength stimuli that produce photopically matched responses in normal subjects elicited a grossly mismatched response in the patient with larger and unusually shaped waveforms in response to the SW stimulus, consistent with the diagnosis of ESCS (Figure 3C). The findings were highly suggestive of ESCS, and gene screening was pursued, which confirmed a previously reported (c.119-2A>C), and a novel (c.119-1G>A), mutations in *NR2E3* segregating in a compound heterozygote state.[3,14] The novel mutation disrupts the same universal “AG” splice acceptor site as the known mutation and can be considered pathogenic.[14] Molecular confirmation led to the discontinuation of the steroid therapy in favor of treatment with topical and systemic carbonic anhydrase inhibitors in the hopes of improving the cystoid maculopathy mainly for his left eye; however· his visual acuity and CME remained unchanged.

Retinal Function and Colocalized Cross-Sectional and Cellular Structure

Short-wavelength automatic static perimetry demonstrated hypernormal S-cone-mediated sensitivities across the central and near midperipheral retina, particularly in nasal retina (Figure 3A). Two-color dark-adapted perimetry confirmed no rod mediation of the stimuli (not shown). The areas with hypersensitivity on perimetry colocalize with areas of the retina with an intact ISe and IZ and a thick ONL on OCT (Figure 3B). The ONL at two locations at 0.8 mm and 1.9 mm in the temporal retina is twice the normal thickness. The decline in S-cone sensitivity in the temporal retina colocalizes with the locations where the ISe band becomes undetectable.

AOSLO imaging was used to explore the cone photoreceptor mosaic. Cone density is approximately 2-fold and 3-fold higher than normal in the patient at 0.8 mm and 1.9 mm temporal to the fovea, respectively. The greater than normal cone densities in regions with S-cone hypersensitivity in this patient suggest the cone mosaic is enriched with supernumerary S-cones. The ESCS cone outer segment waveguided signals appear smaller than normal eccentricity-matched waveguided reflectance from normal cones. We approached this quantitatively by examining the intercone spacing in the patient with ESCS compared with normal. Intercone spacing in the patient with ESCS was 74% and 56% of normal cone spacing at 0.8 mm and 1.8 mm temporal.[21] This intercone spacing is smaller than the normal cone inner segment diameter at comparable retinal locations (6.3 and 7.2 μm at 0.8 and 1.8 mm temporal, respectively), suggesting that the cones in the patient with ESCS are necessarily smaller than normal.

Discussion

Inherited retinal degenerations can show signs that overlap with those caused by intermediate uveitis and autoimmune retinopaties.[17,22] Autoimmune and/or inflammatory processes secondary to these molecularly heterogeneous degenerations may explain the clinical overlap and have been implicated in the pathophysiology.[17,22] Cystoid macular edema, the most common overlapping sign, occurs frequently in patients with IRD at some timepoint in the course of their disease and may be more prevalent in specific molecular subtypes, such as autosomal dominant retinitis pigmentosa caused *rhodopsin* class A mutations, *CRB1*- and ESCS-associated IRDs, and Usher syndrome.[1,10,20,22] Vascular sheathing, vitreous degeneration, and cellular vitreous are also frequently described.[17] *CRB1*-associated IRD and ESCS present diagnostic dilemmas as the retina may be thick, in some cases with CME, vitreal changes, and leakage on fluorescein angiography.[23]

Strong evidence supports the use of carbonic anhydrase inhibitors in IRDs in general, and in ESCS in particular, although the indications for treatment should be based on vision rather than the retinal appearance as the changes may represent an abnormal intercellular environment rather incompetence of the inner and outer blood-retinal barriers.[10,11] Of course, immunosuppression or immunomodulation are alternatives that should be carefully considered should there be a failure with the use of carbonic anhydrase inhibitors in the presence of vision loss attributable to CME and after other causes of macular edema, such as choroidal neovascularization, have been ruled out.[15]

NR2E3 plays a critical role in photoreceptor differentiation.[4] A model has been proposed whereby *NR2E3* suppresses cone-specific genes in postmitotic, NRL-expressing, early rod photoreceptor precursors and commits these cells to a rod fate rather than to the default S-cone phenoptype.[4] Consistent with this mechanism, ESCS caused by mutations in *NR2E3* results in supernumerary S-cones that appear to be distributed after the normal rod photoreceptor topography.[6,8,24] The opportunity presented to examine with AOSLO the cone photoreceptor mosaic of our young patient. We found 2- to 3-fold greater cone densities at a location in temporal parafovea with borderline hypersensitive S-cones by psychophysics, confirming observations of supernumerary S-cones in patients with ESCS documented ex vivo in two histopathologic reports and of supernumerary cones in vivo with AOSLO.[6,12,24,25] The estimated cone densities (L/M- and S-cones) in our patient were higher than normal, but lower than the total photoreceptor densities (rods and cones) for the eccentricity. This finding suggests the final cone photoreceptor mosaic in ESCS does not result from a programmed conversion of all potential rod precursors into S-cones, but rather of a subset of the initial rod precursors. Alternatively, the number of fated S-cones may be limited by degeneration occurring since their terminal differentiation.[26] Interestingly, the cone outer segment signals from our patient appeared smaller in diameter than eccentricity-matched waveguided reflectance signals of normal cones. Intercone spacing was reduced up to half the normal spacing, which was also smaller than normal cone inner segment diameters at comparable retinal locations, suggesting that cones in this patient with ESCS are necessarily smaller than normal. We speculate that the finding may reflect the existence of a “hybrid” phenotype of “S-cones” with outer segments that are smaller in size than normal cones, although larger than rods, analogous to observations in the *rd7* mouse model of the disease.[26,27] Alternatively, the mosaic may represent cross-sections of slender S-cone cone outer segment tips imaged more distally than neighboring (more vitread) L-M cones.[28] Greater differences in size between rods and cones near the ellipsoid region of the inner segment may be exploited as morphometric markers to help clarify this finding.[27,28] Imaging of the cone inner segments by nonconfocal split-detection AOSLO imaging in our patient, however, failed to reveal the boundaries between neighboring cone inner segments, perhaps in part because of the high cone densities measured.[21] The finding also suggested the changes may not be limited to S-cones but rather to the entire cone photoreceptor mosaic. The use of imaging techniques that separate cone photoreceptor subtypes may help clarify the significance of these signals.[29] Changes in waveguiding or reflective properties of cones as a result of the primary developmental abnormality or as a consequence of degeneration may contribute to the apparent smaller than normal cone outer segment diameters in our patient.

Enhanced S-cone syndrome is a slowly progressive condition, and the sequence of events that lead to degeneration is still not completely understood but likely includes disruption of developmental and postnatal maintenance processes.[6,8] The documentation of a relatively well-laminated central retina and of a relatively well-organized cone photoreceptor mosaic in the patient reported herein as well as in other young patients with ESCS, however, raises hope that emerging therapies may be able to abort the onset of degenerative changes and perhaps even revert some of the functional abnormalities.

Acknowledgment

The authors thank Alfredo Dubra. Funding support from Foundation Fighting Blindness (C-CL-0913-0626-UPA01; C-GT-0913-0628-UPA03), Research to Prevent Blindness Stein Innovation Award, and National Eye Institute, National Institutes of Health (NEI, NIH) (P30 EY001583, U01 EY025477, and R01 EY028601), the F. M. Kirby Foundation; and the Paul and Evanina Mackall Foundation Trust.

References

1. Marmor M, Jacobson S. Diagnostic clinical findings of a new syndrome with night blindness, maculopathy, and enhanced S cone sensitivity. Am J Ophthalmol 1990;110:124–134. [PubMed: 2378376]
2. Swaroop A, Xu JZ, Pawar H, et al. A conserved retina-specific gene encodes a basic motif/leucine zipper domain. Proc Natl Acad Sci U S A 1992;89:266–270. [PubMed: 1729696]
3. Haider NB, Jacobson SG, Cideciyan AV, et al. Mutation of a nuclear receptor gene, NR2E3, causes enhanced S cone syndrome, a disorder of retinal cell fate. Nat Genet 2000;24:127–131. [PubMed: 10655056]
4. Swaroop A, Kim D, Forrest D. Transcriptional regulation of photoreceptor development and homeostasis in the mammalian retina. Nat Rev Neurosci 2010;11:563–576. [PubMed: 20648062]
5. Littink K, Stappers P, Riemslag F, et al. Autosomal recessive NRL mutations in patients with enhanced S-cone syndrome. Genes 2018;9:68.
6. Milam AH, Rose L, Cideciyan AV, et al. The nuclear receptor NR2E3 plays a role in human retinal photoreceptor differentiation and degeneration. Proc Natl Acad Sci U S A 2002;99:473–478. [PubMed: 11773633]
7. Hull S, Arno G, Sergouniotis PI, et al. Clinical and molecular characterization of enhanced S-cone syndrome in children. JAMA Ophthalmol 2014;132:1341–1349. [PubMed: 25079116]
8. Garafalo AV, Calzetti G, Cideciyan AV, et al. Cone vision changes in the enhanced S-cone syndrome caused by *NR2E3* gene mutations. Investig Opthalmol Vis Sci 2018;59:3209.
9. Audo I, Michaelides M, Robson AG, et al. Phenotypic variation in enhanced S-cone syndrome. Invest Ophthalmol Vis Sci 2008;49:2082–2093. [PubMed: 18436841]
10. Salvatore S, Fishman GA, Genead MA. Treatment of cystic macular lesions in hereditary retinal dystrophies. Surv Ophthalmol 2013;58:560–584. [PubMed: 24160730]
11. Sharon D Shared mutations in NR2E3 in enhanced S-cone syndrome, goldmann-favre syndrome, and many cases of clumped pigmentary retinal degeneration. Arch Ophthalmol 2003;121:1316. [PubMed: 12963616]
12. Park SP, Hong IH, Tsang SH, et al. Disruption of the human cone photoreceptor mosaic from a defect in NR2E3 transcription factor function in young adults. Graefes Arch Clin Exp Ophthalmol 2013;251:2299–2309. [PubMed: 23604511]
13. Wright AF, Reddick AC, Schwartz SB, et al. Mutation analysis of NR2E3 and NRL genes in enhanced S cone syndrome. Hum Mutat 2004;24:439.
14. Yzer S, Barbazetto I, Allikmets R, et al. Expanded clinical spectrum of enhanced S-cone syndrome. JAMA Ophthalmol 2013;131:1324–1330. [PubMed: 23989059]
15. Hood DC, Cideciyan AV, Roman AJ, Jacobson SG. Enhanced S cone syndrome: evidence for an abnormally large number of S cones. Vis Res 1995;35:1473–1481. [PubMed: 7645276]
16. Jacobson SG, Sumaroka A, Aleman TS, et al. Nuclear receptor NR2E3 gene mutations distort human retinal laminar architecture and cause an unusual degeneration. Hum Mol Genet 2004;13:1893–1902. [PubMed: 15229190]
17. Yoshida N, Ikeda Y, Notomi S, et al. Clinical evidence of sustained chronic inflammatory reaction in retinitis pigmentosa. Ophthalmology 2013;120:100–105. [PubMed: 22986109]
18. Jacobson SG, Voigt WJ, Parel JM, et al. Automated light- and dark-adapted perimetry for evaluating retinitis pigmentosa. Ophthalmology 1986;93:1604–1611. [PubMed: 3808619]
19. Morgan JIW, Vergilio GK, Hsu J, et al. The reliability of cone density measurements in the presence of rods. Transl Vis Sci Technol 2018;7:21.

20. Aleman TS, Cideciyan AV, Sumaroka A, et al. Retinal laminar architecture in human retinitis pigmentosa caused by Rhodopsin gene mutations. Invest Ophthalmol Vis Sci 2008;49:1580–1590. [PubMed: 18385078]
21. Scoles D, Sulai YN, Langlo CS, et al. In vivo imaging of human cone photoreceptor inner segments. Investig Opthalmology Vis Sci 2014;55:4244.
22. Heckenlively JR, Aptsiauri N, Nusinowitz S, et al. Investigations of antiretinal antibodies in pigmentary retinopathy and other retinal degenerations. Trans Am Ophthalmol Soc 1996;94:179–200; discussion 200–206. [PubMed: 8981696]
23. Aleman TS, Cideciyan AV, Aguirre GK, et al. Human CRB1-associated retinal degeneration: comparison with the rd8 Crb1-mutant mouse model. Invest Ophthalmol Vis Sci 2011;52:6898–6910. [PubMed: 21757580]
24. Bonilha VL, Fishman GA, Rayborn ME, Hollyfield JG. Retinal pathology of a patient with goldmann-favre syndrome. Ophthalmic Genet 2009;30:172–180. [PubMed: 19852574]
25. Roorda A, Sundquist S, Solovyev A, et al. Adaptive optics imaging reveals supernormal cone density in enhanced S-cone syndrome. Invest Ophthalmol Vis Sci 2010;51:2934.
26. Cheng H, Khan NW, Roger JE, Swaroop A. Excess cones in the retinal degeneration rd7 mouse, caused by the loss of function of orphan nuclear receptor Nr2e3, originate from early-born photoreceptor precursors. Hum Mol Genet 2011;20:4102–4115. [PubMed: 21813656]
27. Corbo JC, Cepko CL. A hybrid photoreceptor expressing both rod and cone genes in a mouse model of enhanced S-cone syndrome. PLoS Genet 2005;1:e11. [PubMed: 16110338]
28. Calkins DJ. Seeing with S cones. Prog Retin Eye Res 2001;20:255–287. [PubMed: 11286894]
29. Sabesan R, Hofer H, Roorda A. Characterizing the human cone photoreceptor mosaic via dynamic photopigment densitometry. PLoS One 2015;10:e0144891. [PubMed: 26660894]

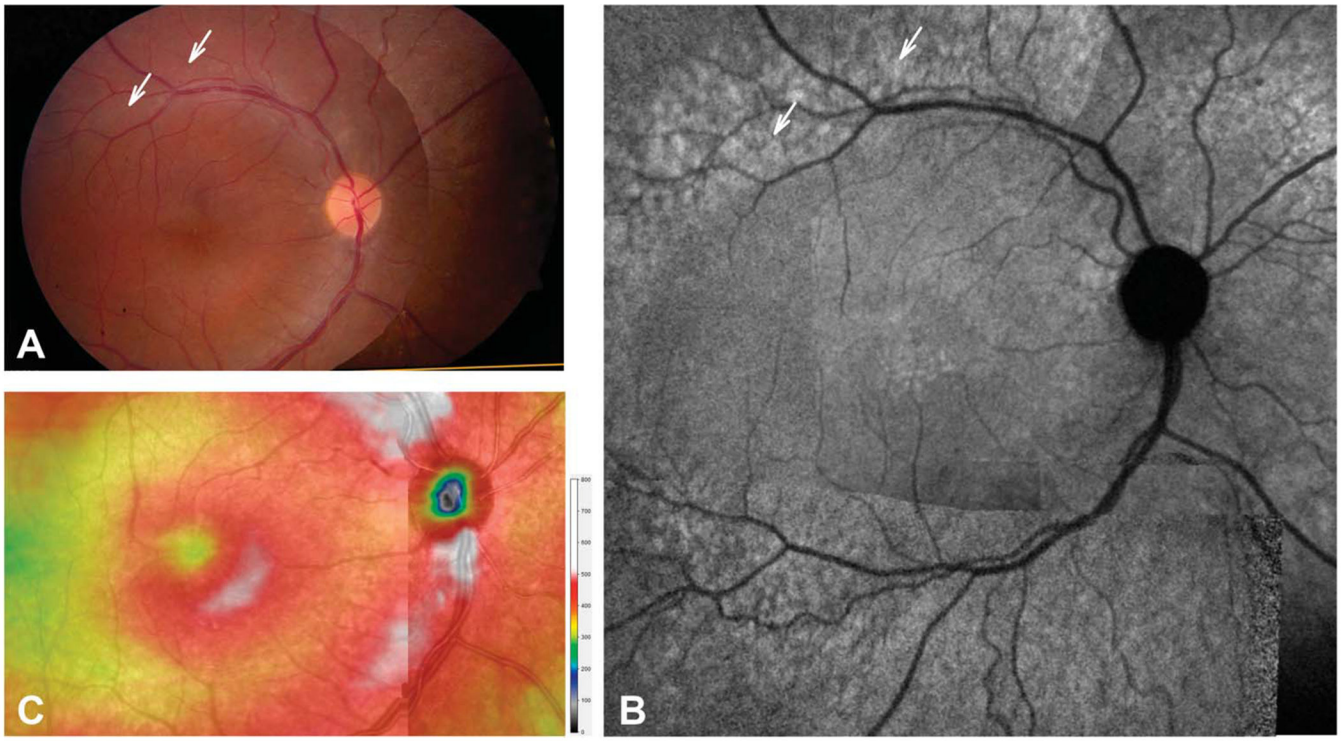

Fig. 1.

En face imaging in the patient. Montages of fundus photographs (**A**), NIR-FAF (**B**), and total retinal thickness topography of the central macula and peripapillary retina (**C**). Arrows (**A** and **B**) point to the retina along the vascular arcades that appears normal on fundus photography but show hyperautofluorescence on NIR-FAF.

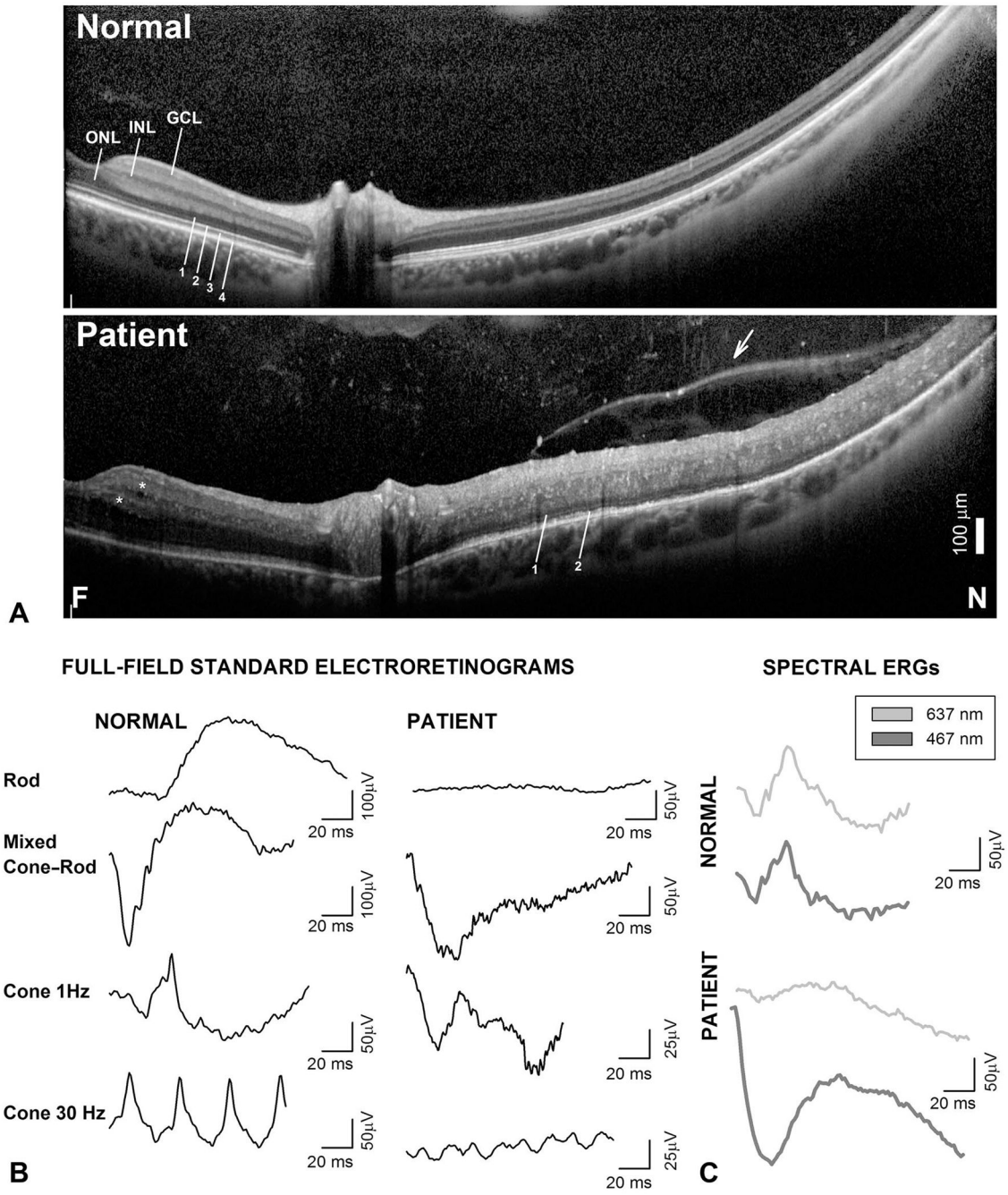

Fig. 2.

Diagnostic hallmarks of ESCS on SD-OCT and full-field ERGs. **A.** Horizontal, 16.4-mm-long, SD-OCT cross-section from near fovea (F) into nasal (N) retina in the patient compared with a normal subject. Nuclear layers (INL, inner nuclear layer; GCL, ganglion cell layer) and outer photoreceptor laminae are labeled (1, outer limiting membrane; 2, inner segment/outer segment junction near the inner segment ellipsoid zone [ISe]; 3, interdigitation between photoreceptor outer segment tips and apical retinal pigment epithelium; and 4, retinal pigment epithelium, following conventional terminology. Asterisks

are placed near hyporreflective cystoid spaces. Arrow points to vitreoretinal band or posterior hyaloid that separates optically empty spaces from a vitreous with reflective dots. **B.** Standard full-field ERGs in the patient compared with a representative normal subject. **C.** Light-adapted ERGs elicited with long-wavelength (637-nm, thin *gray traces*) and SW (467-nm, *thick gray traces*) stimuli matched (3 phot-cd·s·m^{-2}) for L-M cone stimulation in the normal subject elicit grossly mismatched waveforms in the patient. Traces start at stimulus onset. Calibration bars are to the right of the traces.

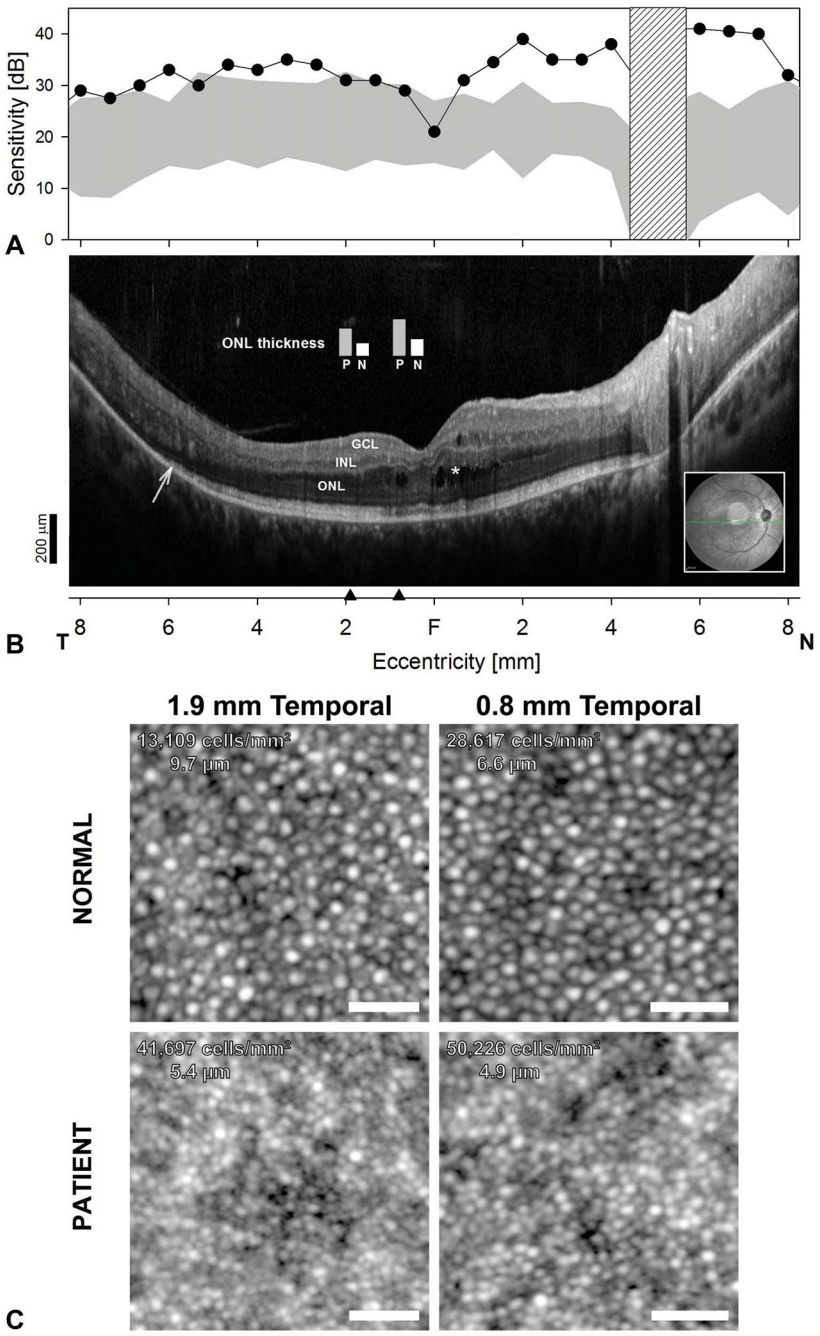

Fig. 3.

A. Central retinal function and colocalized cross-sectional and cellular structure in ESCS. S-cone sensitivity profiles measured with a 440-nm stimulus on a yellow L-M cone adapting background compared with the normal range (gray band = mean ± 2 SD). Hatched bar: blind spot. **B.** Horizontal, 16.5-mm, SD-OCT through the fovea in the patient. Inset is an NIR-REF image with the location and orientation of the scan (*green arrow*). Asterisks denote cystoid spaces. Arrow points to transition zone where the ISe band becomes undetectable. Black arrow heads on the eccentricity axis denote locations where ONL

thickness measurements from the patient (P) were compared with normal measurements (N) (plotted as vertical bars overlaid above SD-OCT cross-section). Scale bar is to the bottom left; (**A** and **B**) share the same eccentricity scale. **C.** AOSLO images from the patient with ESCS compared with a normal. Cone densities and cone spacing are denoted in panel. Cone density is approximately 2- and 3-fold higher than normal in the patient at 0.8 mm and 1.9 mm (~3° and 6°) temporal to the fovea, respectively. Scale bar: 25 μm.